HHS Public Access

Author manuscript

Neuron. Author manuscript; available in PMC 2018 December 06.

Published in final edited form as:

Neuron. 2017 December 06; 96(5): 1013–1023.e4. doi:10.1016/j.neuron.2017.11.014.

Age-dependent effects of apoE reduction using antisense oligonucleotides in a model of β-amyloidosis

Tien-Phat V. Huynh[1,2], **Fan Liao**[1], **Caroline M. Francis**[1], **Grace O. Robinson**[1], **Javier Remolina Serrano**[1], **Hong Jiang**[1], **Joseph Roh**[1], **Mary Beth Finn**[1], **Patrick M. Sullivan**[3], **Thomas J. Esparza**[1], **Floy R. Stewart**[1], **Thomas E. Mahan**[1], **Jason D. Ulrich**[1], **Tracy Cole**[4], and **David M. Holtzman**[1,5,*]

[1]Department of Neurology, Hope Center for Neurological Disorders, Knight Alzheimer's Disease Research Center, Washington University School of Medicine, St. Louis, MO 63110, USA

[2]Medical Scientist Training Program (MSTP), Washington University School of Medicine, St. Louis, MO 63110, USA

[3]Department of Medicine, Duke University Medical Center, Durham Veterans Health Administration Medical Center's Geriatric Research, Education and Clinical Center, Durham, NC 27710, USA

[4]Ionis Pharmaceuticals, Inc., 2855 Gazelle Ct. Carlsbad, CA 92024, USA

Summary

The apolipoprotein E (*APOE*) gene is the strongest genetic risk factor for late-onset Alzheimer disease. Previous studies suggest reduction of apoE levels through genetic manipulation can reduce Aβ pathology. However, it is not clear how reduction of apoE levels after birth would affect amyloid deposition. We utilize an antisense oligonucleotide (ASO) to reduce apoE expression in the brains of APP/PS1-21 mice homozygous for the APOE-ε4 or APOE-ε3 allele. ASO treatment starting after birth led to a significant decrease in Aβ pathology when assessed at 4 months. Interestingly, ASO treatment starting at the onset of amyloid deposition led to an increase in Aβ plaque size and a reduction in plaque-associated neuritic dystrophy with no change in overall plaque load. These results suggest that lowering apoE levels prior to plaque deposition can strongly affect the initiation of Aβ pathology while lowering apoE after Aβ seeding modulates plaque size and toxicity.

eTOC Blurb

[*]Correspondence: holtzman@wustl.edu.
[5]Lead Contact

Author Contributions

T-P.V.H., T.C. J.D.U., and D.M.H. conceived and designed the project. T-P.V.H., J.D.U., and D.M.H. wrote the paper. T-P.V.H. performed most of the experiments, assisted by F.L., C.M.F., G.O.R., J.S., H.J., J.R., M.B.F., T.J.E., F.R.S., and T.E.M. T-P.V.H., F.L., C.M.F., J.D.U., and D.M.H. analyzed the data. P.M.S. provided the *APOE-KI* mice. T.C. designed and provided the ASO. All authors read and commented on the manuscript.

Huynh et al. demonstrated that apoE3 and apoE4 are critical factors in promoting amyloidosis during the early stages of Aβ plaque formation, but not during the exponential growth phase. Importantly, reduction of apoE4 decreases neuritic dystrophy independent of Aβ pathology.

Introduction

Alzheimer disease (AD) is the most common cause of dementia. Two main proteins accumulate in the brain in aggregated forms in AD; amyloid-β (Aβ) and tau. Aβ accumulation in extracellular amyloid plaques consists mostly of aggregated forms of Aβ. Apolipoprotein E (apoE) was found to co-localize with amyloid plaques (Namba et al., 1991), and the *APOE* gene was identified as the strongest genetic risk factor for late-onset AD (Strittmatter et al., 1993). The human *APOE* gene contains two single-nucleotide polymorphisms (SNPs) that result in three most common variants: ε2 (cys112, cys158), ε3 (cys112, arg158), and ε4 (arg112, arg158). Individuals with one copy of the ε4 allele have a 3.7-fold and two copies a 12-fold increased risk of developing AD relative to the ε3/ε3 genotype (Bertram et al., 2007). ApoE strongly influences AD pathology via its effects on Aβ metabolism, promoting Aβ aggregation (Ma et al., 1994; Wisniewski et al., 1994) and impairing its clearance from the brain interstitial fluid in an isoform-dependent fashion (Castellano et al., 2011; Deane et al., 2008). Studies in APP/PS1 transgenic mice hemizygous for either human *APOE4* or *APOE3* showed that germ-line reduction of apoE levels decreases Aβ pathology (Bien-Ly et al., 2012; Kim et al., 2011). For mechanistic and therapeutic implications, we investigated whether lowering apoE before and after the onset of Aβ pathology would have beneficial effects on Aβ deposition and other phenotypes. To this end, we utilized an anti-sense oligonucleotide (ASO) that specifically and effectively lowers apoE expression by more than 50% in the brains of APP/PS1-21 mice that are homozygous for either the human ε4 or ε3 allele. When ASO treatment was started at post-natal day (P) 0, we observed a significant reduction in Aβ pathology at 16 weeks of age for mice expressing either apoE isoform. Interestingly, no significant effect on overall Aβ levels in the brain of either cohort were detected when the treatment was initiated at 6 weeks of age and assessed at 16 weeks. Importantly, ASO treatment led to a significant reduction in plaque-associated neuritic dystrophy in both P0- and 6-week-treated (6wk) mice. Our data suggest that apoE level plays a critical role in the early stages of plaque formation but the effects are much more limited in the presence of Aβ pathology. However, apoE reduction maybe effective in reducing plaque-associated toxicity, independent of plaque load.

Results

Treatment with ASO effectively reduces *APOE* expression *in vivo*

To assess the efficacy of the anti-apoE ASO (hereon referred to as ‘ASO’) and determine the optimal dose, APOE3/3 and APOE4/4-knock-in (E3KI and E4KI) mice were subjected to intracerebroventricular (ICV) treatment strategies with varying doses and durations (Figure 1A). Three-month-old (mo) E3KI and E4KI mice received unilateral ICV injection with either ASO, control ASO (cASO), or PBS (vehicle control). cASO has the same length and chemical modifications as the ASO, but is not specific for any known sequence in mouse. A total bolus of 350 μg or 500 μg of either ASO or cASO was injected into the right lateral

ventricle. A third cohort was treated with PBS to control for any toxicity associated with the ASO. Following a 2-week incubation, we assessed apoE mRNA and protein expression in the hippocampus and cortex. ASO treatment reduced apoE mRNA and protein levels by at least 50% relative to controls when assessed through qPCR (Figure 1C) and ELISA (Figure 1D). ApoE reduction was also evident by Western blot (WB) analysis (Figure 1E). Similar knock-down of apoE was also seen in the contralateral hippocampus (Figure S1D and S1E) and cortex (data not shown). The same ASO showed similar efficacy in E3KI mice (Figure S1F–H).

For newborn pups, the optimal dosage used in the adult mice was adjusted relative to weight (mg/kg). PBS or 32 μg of ASO dissolved in PBS was injected into the right lateral ventricle of P0 pups. cASO was not included in the P0 cohort due to lack of any noticeable toxicity or modulation of apoE levels in the adult cohort. PBS-soluble apoE levels in the ipsilateral cortex were significantly reduced (~40–50%) at 1 month (Figure S1B) and 2 months (Figure 1B). There was also a significant reduction of soluble apoE in the contralateral cortex at 2 months (Figure S1C).

To assess the effect of lowering apoE on amyloidosis, we crossed APP/PS1-21 mice with either E4KI or E3KI mice to obtain APP transgenic mice on an *APOE4/4* or *APOE3/3* background (APPE4 and APPE3 mice, respectively) (Kim et al., 2011; Radde et al., 2006). To investigate whether the timing of apoE reduction affected the outcome, we began ASO treatment at two time points: P0 and 6 weeks of age (i.e. onset of plaques in the neocortex). A booster dose was given midway through the duration for both cohorts to maintain sufficient knockdown of apoE levels (Figure 1F).

Animals in the 6wk cohort received a 350-μg bolus of either ASO, cASO, or PBS through unilateral ICV injections. In ELISA analysis of soluble brain lysates from the contralateral cortex of APPE4 mice, there was a significant reduction (≥ 50%) of apoE in the ASO-treated mice relative to either control groups at the end of the treatment period (Figure 1I). Similar treatment of APPE3 mice yielded similar levels of apoE reduction (Figure S1K).

For the P0 cohort, 32 μg of ASO or PBS was injected ICV into the right hemisphere of APPE4 or APPE3 pups at P0. Since the cASO did not modulate apoE levels in the 6wk animals, we did not include a cASO group in this cohort. A booster dose of 350 μg ASO or PBS was given at 8 weeks of age (Figure 1F). At the end of the treatment period (4 mo), significant reduction of soluble apoE was observed in the contralateral cortex in both APPE4 (Figure 1G) and APPE3 mice (Figure S1I).

ASO treatment effectively reduced PBS-soluble apoE protein levels by ~40 – 50% for the entirety of the treatment duration in both cohorts. There were no significant changes in apoE level in the guanidine-soluble (Guan) brain lysates of 4-mo APPE4 mice treated at P0 (Figure 1H) or 6 weeks (Figure 1J). In 4-mo APPE3 mice, a small reduction of Guan apoE was detected in brain lysates of mice treated with ASO starting at P0 (Figure S1J), but not when treatment was started at 6 weeks (Figure S1L).

Although the majority of apoE in the brain is secreted by astrocytes (Pitas et al., 1987), microglia also secrete apoE. We qualitatively examined the cellular uptake of ASOs by

astrocytes (Kordasiewicz et al., 2012) and microglia by co-staining brain sections with their respective markers (GFAP and IBA1), along with a pan-ASO antibody. Co-localization analyses suggest that ASOs are taken up by both microglia and astrocytes in APPE4 (Figure 1K) and APPE3 brains (data not shown).

ASO treatment at P0 significantly reduces Aβ plaque pathology

We first assessed Aβ deposition in the P0-treated APPE4 mice by immunostaining with an anti-Aβ antibody HJ3.4. (Figure 2A,B). We found a significant reduction (~50%) in the area covered by Aβ plaques in ASO-treated mice (Figure 2C). We next quantified fibrillar plaque load using X-34 dye and found a significant reduction of ~50% in the ASO group (Figure 2D,E). In APPE3 mice that underwent the same treatment (Figures S2B,D), a significant reduction of X-34-positive plaques was detected in ASO-treated mice (Figure S2E). Interestingly, there was no significant difference in Aβ-immunoreactive plaques (Figure S2C).

Next, we biochemically assessed $A\beta_{40}$ and $A\beta_{42}$ levels in PBS (soluble) and Guan (insoluble) brain lysates. ASO treatment led to significant reductions of both soluble $A\beta_{40}$ and $A\beta_{42}$ (Figure 2F and 2H) in APPE4 mice. We detected no significant difference in oligomeric Aβ levels between the two treatment groups in APPE4 (Figure 2J) or APPE3 (Figure S2J) cohorts. There was a significant decrease in insoluble $A\beta_{40}$ in the ASO group relative to the PBS group (Figure 2G). While not statistically significant, there was a similarly strong trend towards a reduction of insoluble $A\beta_{42}$ (Figure 2I). Biochemical analyses of brain lysates from the contralateral cortex of P0-treated APPE3 mice found significant reductions of insoluble $A\beta_{40}$ (Figure S2G) and $A\beta_{42}$ (Figure S2I) in the ASO group. No significant differences of either Aβ40 (Figure S2F) or Aβ42 (Figure S2H) were detected in the soluble fraction.

We next investigated the degree of neuritic dystrophy on a per-plaque basis by co-staining brain sections from P0-treated APPE4 mice with X-34 and LAMP1, a marker of dystrophic neurites (Figure 2K) (Gowrishankar et al., 2015). ASO-treated mice had a significant reduction in the volume of dystrophic neurites/plaque, independent of plaque size or plaque load (Figure 2L).

To investigate if the reduction in Aβ pathology was due to altered metabolism of APP we performed WB analyses for APP and C99 (a C-terminal fragment of APP that is generated upon cleavage of APP by β-secretase to generate Aβ). Using antibodies 6E10 and 82E1 to detect APP and C99, respectively, we did not detect a difference in the levels of these proteins in RIPA-soluble brain lysates from APPE4 mice treated with PBS or ASO at P0 (Figure S2L). Similarly, ASO treatment at P0 did not result in altered APP or C99 levels in RIPA-soluble brain lysates from APPE3 mice (Figure S2K). Thus, the reduction in Aβ pathology upon ASO treatment likely results from alterations in other pathways that influence Aβ metabolism.

Reduction of apoE expression starting at 6 weeks of age did not significantly alter total Aβ levels

To assess the effect of reducing apoE at the onset of Aβ accumulation (Figure 3A), we performed Aβ immunostaining on brain sections from 4-mo APPE4 mice treated with either PBS, ASO, or cASO starting at 6 weeks of age (Figure 3B). Analyses of the area covered by Aβ staining showed a significant increase in the ASO treatment group relative to either control groups (Figure 3D). To further characterize the nature of the deposited Aβ plaques, brain sections were stained with X-34 (Figure 3C). Quantitative analyses of X-34-stained areas showed no statistically significant difference among treatment groups (Figure 3E). Histological analyses of brain sections from the 6wk cohort of APPE3 mice yielded no significant differences among any treatment group in the percentage of area stained with either an anti-Aβ antibody (Figure S3B and S3D) or X-34 dye (Figure S3C and S3E).

Next, we analyzed total Aβ levels biochemically from cortices of APPE4 mice in the 6wk cohort and found a small (~20%) reduction of insoluble $A\beta_{40}$ level in the ASO-treated mice compared to the PBS-treated mice (Figure 3G). However, there was no significant difference in insoluble $A\beta_{42}$ levels among any treatment groups (Figure 3I). No dramatic differences in $A\beta_{40}$ or $A\beta_{42}$ among any treatment groups were detected in the soluble fraction, although there was a slight, albeit statistically significant increase in $A\beta_{42}$ levels in ASO compared to PBS-treated groups (Figure 3F and 3H). These results suggest that, while ASO treatment starting at 6 weeks of age did not significantly lower the amount of total Aβ deposition, there are some subtle changes within the different Aβ pools as well as in the types of plaques. Similar analyses in the 6wk cohort of APPE3 mice revealed a significant reduction of insoluble $A\beta_{40}$, but not $A\beta_{42}$, in the ASO group compared to either controls (Figure S3G and S3I, respectively). No changes in soluble $A\beta_{40}$ (Figure S3F) or $A\beta_{42}$ (Figure S3H) were observed.

To determine whether the ASO treatment altered the degree of neuritic dystrophy, we performed co-staining of brain sections from the 6wk cohort of APPE4 mice with X-34 and LAMP1 (Figure 3J). When the volume of LAMP1-positive areas within 15 μm of an $X\text{-}34^+$ plaque was quantified (normalized to the volume of X-34), we found the ASO-treated mice to have significantly less dystrophic neurites compared to PBS-treated mice, despite a lack of overall effect on plaque load. (Figure 3K).

The lipidation state of apoE affects Aβ accumulation in some models of amyloidosis (Huynh et al., 2017). Thus, we investigated whether ASO treatment altered the lipidation state of apoE. CSF collected from APPE4 and APPE3 mice across all treatment groups were subjected to native gel analysis for apoE lipidated particles (Ulrich et al., 2013). No significant shift in the size or distribution of the apoE particles among treatment groups in APPE4 (Figure S3K) or APPE3 (Figure S3J) mice was observed.

ASO treatment alters plaque size distribution

To examine the increase in Aβ deposition in the 6wk cohort of ASO-treated APPE4 mice, we analyzed the plaques (Figure 4A) by grouping individual plaques based on size in bins of 326 μm^2 per increment, and the total area covered by each bin was plotted on the y-axis to

obtain an overall size distribution. We first analyzed the data obtained from anti-Aβ staining (Figure 4B and 4C). We detected a significant shift in the size distribution of the plaques between the ASO and control groups. Analysis of the frequency of each size-group revealed an increase in the number of the larger (> 694 μm^2) plaques in the ASO group relative to the control groups (figure 4C, bottom panel). Correspondingly, the total area covered by the larger plaques was increased in the ASO group (Figure 4C, top panel), which was accompanied by an increase in both plaque density and average plaque size in the ASO group (Figure 4F and 4G, respectively). These findings were confirmed using another anti-Aβ antibody, 82E1 (Figure S4B). Quantitative analyses found an increase in percent area coverage of Aβ-stained plaques (Figure S4D), as well as the number of plaques larger than 694 μm^2 (Figure S4C). This shift is driven by both an increase in plaque density (Figure S4E) and average plaque size (Figure S4F). Interestingly, plaque size analysis on Aβ-immunostained sections from APPE3 mice yielded very similar findings. We found significant differences in cumulative distribution between the cASO and ASO groups, as well as between the PBS and ASO groups, but not between the cASO and PBS groups (Figure S4H). This shift in plaque size distribution is primarily driven by an increase in average plaque size (Figure S4K), but not plaque density (Figure S4J).

We performed similar analyses on the X-34-stained dataset from APPE4 brain sections (Figure 4D and 4E). While we did not find a significant shift in cumulative distribution of plaque size, we found a significant decrease in plaque density in the ASO group relative to either control groups (Figure 4H), and no change in average plaque size (Figure 4I). A frequency analysis suggests this decrease in density might be due to a decrease in smaller (< 1020 μm^2) plaques (Figure 4E, bottom panel). Similar analyses performed on the X-34-stained brain sections from 6wk APPE3 mice found a significant shift in plaque size distribution between the ASO and PBS groups, but not between the ASO and cASO, or between the cASO and PBS groups (Figure S4I). No changes in plaque density (Figure S4L) or average plaque size (Figure S4M) were detected.

Altered microglial responses are associated with changes in plaque load and plaque properties. To probe for any changes in the microglial response in the 6wk cohort, we performed histological staining for CD45, a marker of activated microglia. Plaque-associated microglial activation was evident around Aβ deposits in APPE4 (Figure 4J) and APPE3 (Figure S4N) mice. Analysis of $CD45^+$ area did not detect any significant differences between treatment groups in APPE4 (Figure 4K) or APPE3 (Figure S4O) mice.

Discussion

Aβ aggregation is amongst the earliest detectable pathologies in AD. Identifying methods to reduce the formation of Aβ plaques has been the goal of preclinical and clinical studies. In this study, we examined the effects of postnatal apoE reduction in APPE4 or APPE3 mice using an anti-apoE ASO. ASO treatment starting at P0 led to a significant reduction in Aβ pathology regardless of apoE isoform. However, when ASO treatment was initiated at the onset of Aβ aggregation in the brain, no major change in amyloid burden was detected. These results suggest that both apoE4 and apoE3 promote the initial nucleation of Aβ plaques, but do not exert a strong effect on the subsequent growth of plaques. This latter

point is important to address in lieu of recent clinical observations that AD pathology occurs and progresses decades prior to symptom onset (Jack and Holtzman, 2013). Consistent with previous *in vivo* studies (Fryer et al., 2005; Holtzman et al., 2000), apoE4 is more potent as a pro-amyloidogenic agent as our data showed the total levels of Aβ accumulation in APPE4 brains to be consistently higher than in APPE3 brains. Notably, we observed a marked decrease in neuritic dystrophy around the plaques in APPE4 mice treated with ASO under either treatment paradigm, independent of plaque size or plaque load. This suggests a general role of apoE4 in modulating the brain's response to neurotoxic insults (i.e. Aβ plaques), independent of its effects on Aβ.

The different outcomes between the P0 and 6wk treatment cohorts likely result from the 6-week delay in the initiation of treatment, rather than the difference in treatment duration. This developmental window likely corresponds to the period just prior to the "lag phase" in the *in vitro* Aβ aggregation model, where monomers aggregate to form oligomers (Jarrett and Lansbury, 1993). Aβ oligomers have been proposed to act as nuclei that facilitate rapid fibrillization in the exponential "growth phase" (Roychaudhuri et al., 2009). While no Aβ deposits can be detected in these mice until ~2 mo, it is likely that oligomeric Aβ has already formed in sufficient amount to initiate fibril elongation by 6 weeks of age. It is possible that 6 weeks less exposure to ASO-treatment in the 6wk group could be responsible for the decreased effect on Aβ. However, this seems unlikely given that the effects seen in the 6wk group are clearly present but they are affecting fibrillar vs. non-fibrillar plaque distribution as opposed to Aβ levels. Additional studies are needed to definitively address this issue.

The effects of apoE on soluble Aβ clearance (Castellano et al., 2011; Deane et al., 2008; Verghese et al., 2013) may account in part for reduced Aβ deposition occurring with lower apoE levels in the ASO-treated mice starting at P0. ApoE influences Aβ aggregation *in vitro* (Castano et al., 1995; Ma et al., 1994; Wisniewski et al., 1994) and *in vivo* (Hudry et al., 2013). However, it remained unclear whether apoE exerts its effects in the nucleation or the elongation of plaque, or both. Our data suggest that once Aβ seeding and nucleation occur, further plaque growth is primarily driven by other factors, not apoE levels.

Findings from Liu et al. (published in this issue) utilizing an inducible APOE-overexpression system support this latter hypothesis. Specifically, induction of APOE4 expression in the background of APP_{SWE}/PSΔE9 amyloidosis mice at birth, but not at 6 mo, accelerates plaque deposition. Altogether, data from our study and those from Liu et al. suggest that apoE plays a critical role in the initial formation of Aβ seeds *in vivo* and to a much less extent during the growth period of amyloid plaques.

Though we found no overall change in the microgliosis marker CD45 in the 6wk cohort of either APPE4 or APPE3 mice, the local microglial response could still be altered. Intriguingly, we observed a decrease in neuritic dystrophy immediately around the plaques in both the P0 and 6wk cohorts, independent of plaque size and plaque load. These phenotypes suggest that reduction of apoE4 levels may alter the inflammatory response (i.e. microgliosis) locally, reducing plaque toxicity and dystrophic neurites. This hypothesis is

backed by a growing body of literature suggesting that apoE4 can modulate the inflammatory response in the brain (Huynh et al., 2017).

In summary, we report an *in vivo* study on the effects of apoE-lowering ASO treatment in APPE4 and APPE3 mice. Lowering apoE starting prior to amyloid deposition had a much larger effect on Aβ accumulation as opposed to lowering apoE once Aβ aggregation had already begun. Importantly, reduction of apoE4 at either time point led to a significant reduction in dystrophic neurites, which could reflect on a role of apoE in modulating the brain's response to plaques. These findings carry important implications for *APOE*-targeted therapy, suggesting that treatment would need to start very early, prior to significant amyloidosis in order to achieve maximal effect on plaque load. Alternatively, future studies on the role of apoE in modulating neurotoxicity and the immune system might open up therapeutic options bypassing the need to reduce plaque pathology.

STAR Methods

Contact for Reagent and Resource Sharing

Further information and requests for resources and reagents should be directed to and will be fulfilled by the Lead Contact, David M. Holtzman (holtzman@wustl.edu)

Experimental Model and Subject Details

Generation of human APOE isoform mice with APPswe/PS1(L166P) mutant transgenes—To determine the effect of human apoE3 and apoE4 levels on amyloid deposition, we used knock-in mouse models in which the endogenous murine *Apoe* gene is replaced with either the *APOE3* or *APOE4* gene (Sullivan et al., 1997). APPPS1-21 mice overexpress a human APP cDNA with a Swedish mutation (KM670/671NL) and mutant PS1 with the L166P mutation. Breeding pairs were obtained from Dr. Mathias Jucker, University of Tübingen, Tübingen, Germany (Radde et al., 2006). To replace the murine *Apoe* gene with human *APOE* isoforms, APPPS1-21 mice were bred with either APOE3/E3 or APOE4/4 knock-in mice. APPPS1-21/APOE4/Apoe mice and APOE4/Apoe mice from the first generation were bred with each other to generate APPPS1-21/APOE4/4 and APOE4/4 mice. APPPS1-21/APOE4/4 and APOE4/4 mice were then bred to generate more APPPS1-21/APOE4/4 mice. Similar breeding schemes were followed to generate APPPS1-21/APOE3/3 mice All mice used in this study were maintained on a C57BL/6J background. Mice were subjected to experiments at either P0, 1.5 months, or 3 months of age, per the various experimental designs. Mice were individually housed in AAALAC accredited facilities with temperature and humidity controls, and were under a 12-hours light/dark cycle (lights on at 6:00 AM) cycle with free access to food and water *ad libitum* throughout all phases of the experiments. Males and females animals were used in all experiments at roughly equal ratio. APPPS1-21/APOE4/4 and APPPS1-21/APOE3/3 mice were subjected to experimental conditions beginning at P0 and 6 weeks of age, and sacrificed at 16 weeks of age. APOE4/4 and APOE3/3 mice were subjected to experimental conditions beginning at 3 – 4 months of age, and sacrificed two weeks later. All animal procedures were approved by the Institutional Animal Care and Use Committee (IACUC) at

Washington University, and were in agreement with the Association for Assessment and Accreditation of Laboratory Animal Care (AAALAC, WUSM).

Method Details

ASOs—The ASOs were designed and synthesized by Ionis Pharmaceuticals as described previously (Cheruvallath et al., 2003; McKay et al., 1999) and had the following modifications: 5 nucleotides on the 5′- and 3′-termini containing 2′-O-methoxyethyl modifications and 10 unmodified central oligodeoxynucleotides (DeVos and Miller, 2013a) to support RNaseH activity. To improve nuclease resistance and promote cellular uptake, the ASOs had a phosphorothioate backbone (Bennett and Swayze, 2010). ASOs were solubilized in sterile DPBS immediately before injections. ASO sequences were as follow: anti-apoE ASO: GGTGAATCTTTATTAAAC; Control ASO: CCTATAGGACTATCCAGGAA.

Surgical procedures and tissue collection—Bolus injections of ASO into adult mice were performed as previously described (DeVos and Miller, 2013b). Specifically, for the 6-week cohort, 10 μl of ASO dissolved in DPBS at 35 μg/μl was injected into the right lateral ventricle using a Hamilton syringe (model #1701, Hamilton Company). The injection was done at a rate of 1 μl/second and the needle was held in place for 5 minutes following completion of injection. The mice were allowed to completely recover on a warming blanket and then returned to the home cage. The following coordinates were used, relative to bregma: 0.3 mm rostral, 1 mm lateral (right), 2.5 mm ventral. P0 injections were performed under a protocol adapted from Passini et al. (Passini and Wolfe, 2001). Briefly, cryo-anesthetized pups were injected using a 1701N Neuros syringe (Hamilton Company) with 4 μl of DPBS-dissolved ASO at 8 μg/μl or DPBS into the right lateral ventricle at a 90° angle. The injection was done at a rate of 1 μl/second and the needle was held in place for 10 seconds following completion of injection. The pups were allowed to completely recover on a warming blanket and then returned to the home cage. The following coordinates were used, relative to lambda: 1 mm rostral, 1 mm Lateral (right), 2 mm ventral. Upon perfusion with PBS containing 0.3% heparin, the right hemisphere was fixed overnight at 4°C in 4% paraformaldehyde, followed by immersion into 30% sucrose solution for at least 24 hours. The left hemisphere was snap-frozen with dry ice and stored at −80°C.

Histology—Following immersion in sucrose for at least 24 hours, serial coronal sections (50 μm thickness) were collected from frontal cortex to caudal hippocampus (right hemisphere) using a freezing sliding microtome (ThermoFisher). Three hippocampal-containing sections (separated by 300 μm) from the right hemisphere of each brain were stained either with X-34 dye (Styren et al., 2000) to visualize fibrillary plaques, or with biotinylated HJ3.4 (anti-$A\beta_{1–13}$, mouse monoclonal antibody generated in-house) and 82E1 (IBL America # 10323) antibodies to visualize Aβ immunopositive plaques, as described previously (Bero et al., 2012). Activated microglia were immunostained using rat anti-CD45 (Bio-Rad/AbD Serotec # MCA138), followed by biotinylated goat anti-rat IgG secondary antibody (Thermo Fisher Scientific **PA1-84402**). Quantitative analysis of immunopositive staining was performed as described previously (Bero et al., 2011). Briefly, images of immunostained sections were exported with NDP viewer (Hamamatsu Photonics). Using

ImageJ software, images were converted to 8-bit grayscale, thresholded to highlight Aβ-specific staining and analyzed. For analyses of immunofluorescent staining (including LAMP1, GFAP, IBA1, ASO, APOE, X-34, and Aβ), 20X images were acquired on Nikon A1Rsi Confocal Microscope. Random windows containing clusters of plaques are captured, spanning approximately 30 μm of tissue in the z-plane. The images were obtained with steps of 1.5 μm and were analyzed using Imaris software (Bitplane). Briefly, surfaces were created separately for each of the fluorescent channels, and the volume of the corresponding markers were quantified under the same threshold. Each data point represents the average value from three separate tissue sections (300 μm apart) from one single animal. All analyses were done blinded to treatment and genotype. Please see Key Resources Table for specific antibody references.

Real-time qPCR analysis—RNA was extracted from frozen cortical tissue using Trizol (Life Technologies # 15596026) and purified using the RNeasy mine kit (Qiagen # 71404). Reverse transcription was performed using a High-Capacity cDNA Reverse Transcription Kit (Life Technologies). Real-time qPCR was conducted with TaqMan primers (Life Technologies) and the TaqMan Universal PCR Master Mix (Thermo Fisher Scientific # 4304437) using the StepOnePlus machine (Applied Biosystems). Relative gene expression levels in ASO- and control-treated mice were compared using the $\Delta\Delta C_t$ method with Taqman probe for human apoE (Hs00171168_m1). Glyceraldehyde 3-phosphate dehydrogenase (GAPDH) mRNA level was used as a reference (Mm99999915_g1 Gapdh).

Sandwich ELISA—Brain cortices or hippocampi were sequentially homogenized with cold PBS and then the PBS insoluble material with 5M guanidine buffer in the presence of 1X protease inhibitor mixture (Roche). The levels of $A\beta_{x\text{-}40}$ and apoE were measured by sandwich ELISA. For apoE ELISA, HJ15.6 and HJ15.4b (Liao et al., 2015) were used as capture and detection antibodies, respectively. For $A\beta_{x\text{-}40}$ ELISA, HJ2 (anti-$A\beta_{35–40}$) was used as a capture antibody and for $A\beta_{x\text{-}42}$ ELISA, HJ7.4 (anti-$A\beta_{37–42}$) was used as a capture antibody. HJ5.1-biotin (anti-$A\beta_{13–18}$) (Bero et al., 2011; Liao et al., 2015) was used as the detecting antibody for both Aβ ELISAs. ELISA assays for oligomeric Aβ were performed on fresh PBS-soluble brain homogenates as described previously (Esparza et al., 2016).

Western blot analysis—PBS-soluble brain lysates from the sequential homogenization step were analyzed for total protein concentration with a micro BCA kit (Thermo Scientific). 30 μg of proteins from each sample were loaded onto a NU-PAGE 4–12% Bis-Tris 15 well gel (Thermo Fisher Scientific # NP0336BOX) and the gel was run at 150 V for 1.5 hours. The proteins were subsequently dry-transferred onto a PVDF membrane using the ibot2 system (Life Technologies) and blocked with 5% milk in TBS-T. The membrane was incubated with anti-apoE antibody HJ15.7 (Liao et al., 2015) and anti-β-tubulin antibodies to probe for apoE and a loading control, respectively. Donkey Anti-mouse IgG-HRP was used as secondary antibody (Santa Cruz Biotechnology # sc-2096). For assessment of APP and C99 levels, brains were homogenized in detergent-containing buffer (RIPA) and the lysates were analyzed through SDS-PAGE and Western blotting using 6E10 and 82E1 antibodies, respectively. All blots were developed for ~10 seconds using an enhanced

chemiluminescence (ECL) Ultra kit (Lumigen TMA-6) and imaged on the SynGene Imager (BioRad) at the appropriate exposure. Assessment of APOE particles in the CSF were performed as described previously (Ulrich et al., 2013). Briefly, 2 μl of CSF were loaded onto a Novex WedgeWell 4 – 20% Tris-Glycine gel (Life Technologies # XP04205BOX) and was run at 100 V for 24 hours at 4°C. The proteins were subsequently transferred onto a nitrocellulose membrane using the Mini Gel Tank and Mini Blot Module (ThermoFisher). The blot was blocked with 5% milk in TBS-T and probed with the anti-apoE antibody HJ15.7.

Quantification and Statistical Analysis

Statistics—All values are reported as mean ± SEM. A Mann-Whitney U test was used to assess significance between two groups. A one-way ANOVA was used to assess significance between more than two groups, and Bonferroni's post-hoc test was used to test for differences between each of the groups. A two-sample Kolmogorov-Smirnov test was used to compare the cumulative distribution of plaque sizes. All statistical analyses were performed using Prism software (Graphpad). $p < 0.05$ is considered significant for all tests. No statistical analysis was used to determine sample size a priori. The sample sizes chosen are based on those used in previous studies from our laboratory. The number of samples indicates biological replicates as indicated in each of the figure legends.

Supplementary Material

Refer to Web version on PubMed Central for supplementary material.

Acknowledgments

This work was supported by NIH grants R01AG047644 and R01NS034467 (D.M.H.), the JPB Foundation (D.M.H.), the Gilliam fellowship from the Howard Hughes Medical Institute (T-P. V. H.), and NIH MSTP grant T32 GM07200 (T-V.P.H). We thank Dr. Guojun Bu for communicating his findings and suggestions for our manuscript. We thank Dr. Sarah Fritschi for assisting with the illustrations. We are grateful for the suggestions and support from our colleagues in the Holtzman laboratory.

References

Bennett CF, Swayze EE. RNA targeting therapeutics: molecular mechanisms of antisense oligonucleotides as a therapeutic platform. Annual review of pharmacology and toxicology. 2010; 50:259–293.

Bero AW, Bauer AQ, Stewart FR, White BR, Cirrito JR, Raichle ME, Culver JP, Holtzman DM. Bidirectional relationship between functional connectivity and amyloid-beta deposition in mouse brain. The Journal of neuroscience: the official journal of the Society for Neuroscience. 2012; 32:4334–4340. [PubMed: 22457485]

Bero AW, Yan P, Roh JH, Cirrito JR, Stewart FR, Raichle ME, Lee JM, Holtzman DM. Neuronal activity regulates the regional vulnerability to amyloid-beta deposition. Nature neuroscience. 2011; 14:750–756. [PubMed: 21532579]

Bertram L, McQueen MB, Mullin K, Blacker D, Tanzi RE. Systematic meta-analyses of Alzheimer disease genetic association studies: the AlzGene database. Nature genetics. 2007; 39:17–23. [PubMed: 17192785]

Bien-Ly N, Gillespie AK, Walker D, Yoon SY, Huang Y. Reducing human apolipoprotein E levels attenuates age-dependent Abeta accumulation in mutant human amyloid precursor protein transgenic mice. The Journal of neuroscience: the official journal of the Society for Neuroscience. 2012; 32:4803–4811. [PubMed: 22492035]

Castano EM, Prelli F, Wisniewski T, Golabek A, Kumar RA, Soto C, Frangione B. Fibrillogenesis in Alzheimer's disease of amyloid beta peptides and apolipoprotein E. The Biochemical journal. 1995; 306(Pt 2):599–604. [PubMed: 7534068]

Castellano JM, Kim J, Stewart FR, Jiang H, DeMattos RB, Patterson BW, Fagan AM, Morris JC, Mawuenyega KG, Cruchaga C, et al. Human apoE isoforms differentially regulate brain amyloid-beta peptide clearance. Science translational medicine. 2011; 3:89ra57.

Cheruvallath ZS, Kumar RK, Rentel C, Cole DL, Ravikumar VT. Solid phase synthesis of phosphorothioate oligonucleotides utilizing diethyldithiocarbonate disulfide (DDD) as an efficient sulfur transfer reagent. Nucleosides, nucleotides & nucleic acids. 2003; 22:461–468.

Deane R, Sagare A, Hamm K, Parisi M, Lane S, Finn MB, Holtzman DM, Zlokovic BV. apoE isoform-specific disruption of amyloid beta peptide clearance from mouse brain. The Journal of clinical investigation. 2008; 118:4002–4013. [PubMed: 19033669]

DeVos SL, Miller TM. Antisense oligonucleotides: treating neurodegeneration at the level of RNA. Neurotherapeutics: the journal of the American Society for Experimental NeuroTherapeutics. 2013a; 10:486–497. [PubMed: 23686823]

DeVos SL, Miller TM. 2013bDirect intraventricular delivery of drugs to the rodent central nervous system. Journal of visualized experiments: JoVE. :e50326. [PubMed: 23712122]

Esparza TJ, Wildburger NC, Jiang H, Gangolli M, Cairns NJ, Bateman RJ, Brody DL. Soluble Amyloid-beta Aggregates from Human Alzheimer's Disease Brains. Scientific reports. 2016; 6:38187. [PubMed: 27917876]

Fryer JD, Simmons K, Parsadanian M, Bales KR, Paul SM, Sullivan PM, Holtzman DM. Human apolipoprotein E4 alters the amyloid-beta 40:42 ratio and promotes the formation of cerebral amyloid angiopathy in an amyloid precursor protein transgenic model. The Journal of neuroscience: the official journal of the Society for Neuroscience. 2005; 25:2803–2810. [PubMed: 15772340]

Gowrishankar S, Yuan P, Wu Y, Schrag M, Paradise S, Grutzendler J, De Camilli P, Ferguson SM. Massive accumulation of luminal protease-deficient axonal lysosomes at Alzheimer's disease amyloid plaques. Proceedings of the National Academy of Sciences of the United States of America. 2015; 112:E3699–3708. [PubMed: 26124111]

Holtzman DM, Bales KR, Tenkova T, Fagan AM, Parsadanian M, Sartorius LJ, Mackey B, Olney J, McKeel D, Wozniak D, Paul SM. Apolipoprotein E isoform-dependent amyloid deposition and neuritic degeneration in a mouse model of Alzheimer's disease. Proceedings of the National Academy of Sciences of the United States of America. 2000; 97:2892–2897. [PubMed: 10694577]

Hudry E, Dashkoff J, Roe AD, Takeda S, Koffie RM, Hashimoto T, Scheel M, Spires-Jones T, Arbel-Ornath M, Betensky R, et al. Gene transfer of human Apoe isoforms results in differential modulation of amyloid deposition and neurotoxicity in mouse brain. Science translational medicine. 2013; 5:212ra161.

Huynh TV, Davis AA, Ulrich JD, Holtzman DM. Apolipoprotein E and Alzheimer's disease: the influence of apolipoprotein E on amyloid-beta and other amyloidogenic proteins. Journal of lipid research. 2017; 58:824–836. [PubMed: 28246336]

Jack CR Jr, Holtzman DM. Biomarker modeling of Alzheimer's disease. Neuron. 2013; 80:1347–1358. [PubMed: 24360540]

Jarrett JT, Lansbury PT Jr. Seeding "one-dimensional crystallization" of amyloid: a pathogenic mechanism in Alzheimer's disease and scrapie? Cell. 1993; 73:1055–1058. [PubMed: 8513491]

Kim J, Jiang H, Park S, Eltorai AE, Stewart FR, Yoon H, Basak JM, Finn MB, Holtzman DM. Haploinsufficiency of human APOE reduces amyloid deposition in a mouse model of amyloid-beta amyloidosis. The Journal of neuroscience: the official journal of the Society for Neuroscience. 2011; 31:18007–18012. [PubMed: 22159114]

Kordasiewicz HB, Stanek LM, Wancewicz EV, Mazur C, McAlonis MM, Pytel KA, Artates JW, Weiss A, Cheng SH, Shihabuddin LS, et al. Sustained therapeutic reversal of Huntington's disease by transient repression of huntingtin synthesis. Neuron. 2012; 74:1031–1044. [PubMed: 22726834]

Liao F, Zhang TJ, Jiang H, Lefton KB, Robinson GO, Vassar R, Sullivan PM, Holtzman DM. Murine versus human apolipoprotein E4: differential facilitation of and co-localization in cerebral amyloid

angiopathy and amyloid plaques in APP transgenic mouse models. Acta neuropathologica communications. 2015; 3:70. [PubMed: 26556230]

Ma J, Yee A, Brewer HB Jr, Das S, Potter H. Amyloid-associated proteins alpha 1-antichymotrypsin and apolipoprotein E promote assembly of Alzheimer beta-protein into filaments. Nature. 1994; 372:92–94. [PubMed: 7969426]

McKay RA, Miraglia LJ, Cummins LL, Owens SR, Sasmor H, Dean NM. Characterization of a potent and specific class of antisense oligonucleotide inhibitor of human protein kinase C-alpha expression. The Journal of biological chemistry. 1999; 274:1715–1722. [PubMed: 9880552]

Namba Y, Tomonaga M, Kawasaki H, Otomo E, Ikeda K. Apolipoprotein E immunoreactivity in cerebral amyloid deposits and neurofibrillary tangles in Alzheimer's disease and kuru plaque amyloid in Creutzfeldt-Jakob disease. Brain research. 1991; 541:163–166. [PubMed: 2029618]

Passini MA, Wolfe JH. Widespread gene delivery and structure-specific patterns of expression in the brain after intraventricular injections of neonatal mice with an adeno-associated virus vector. Journal of virology. 2001; 75:12382–12392. [PubMed: 11711628]

Pitas RE, Boyles JK, Lee SH, Foss D, Mahley RW. Astrocytes synthesize apolipoprotein E and metabolize apolipoprotein E-containing lipoproteins. Biochimica et biophysica acta. 1987; 917:148–161. [PubMed: 3539206]

Radde R, Bolmont T, Kaeser SA, Coomaraswamy J, Lindau D, Stoltze L, Calhoun ME, Jaggi F, Wolburg H, Gengler S, et al. Abeta42-driven cerebral amyloidosis in transgenic mice reveals early and robust pathology. EMBO reports. 2006; 7:940–946. [PubMed: 16906128]

Roychaudhuri R, Yang M, Hoshi MM, Teplow DB. Amyloid beta-protein assembly and Alzheimer disease. The Journal of biological chemistry. 2009; 284:4749–4753. [PubMed: 18845536]

Strittmatter WJ, Saunders AM, Schmechel D, Pericak-Vance M, Enghild J, Salvesen GS, Roses AD. Apolipoprotein E: high-avidity binding to beta-amyloid and increased frequency of type 4 allele in late-onset familial Alzheimer disease. Proceedings of the National Academy of Sciences of the United States of America. 1993; 90:1977–1981. [PubMed: 8446617]

Styren SD, Hamilton RL, Styren GC, Klunk WE. X-34, a fluorescent derivative of Congo red: a novel histochemical stain for Alzheimer's disease pathology. The journal of histochemistry and cytochemistry: official journal of the Histochemistry Society. 2000; 48:1223–1232. [PubMed: 10950879]

Sullivan PM, Mezdour H, Aratani Y, Knouff C, Najib J, Reddick RL, Quarfordt SH, Maeda N. Targeted replacement of the mouse apolipoprotein E gene with the common human APOE3 allele enhances diet-induced hypercholesterolemia and atherosclerosis. The Journal of biological chemistry. 1997; 272:17972–17980. [PubMed: 9218423]

Ulrich JD, Burchett JM, Restivo JL, Schuler DR, Verghese PB, Mahan TE, Landreth GE, Castellano JM, Jiang H, Cirrito JR, Holtzman DM. In vivo measurement of apolipoprotein E from the brain interstitial fluid using microdialysis. Molecular neurodegeneration. 2013; 8:13. [PubMed: 23601557]

Verghese PB, Castellano JM, Garai K, Wang Y, Jiang H, Shah A, Bu G, Frieden C, Holtzman DM. ApoE influences amyloid-beta (Abeta) clearance despite minimal apoE/Abeta association in physiological conditions. Proceedings of the National Academy of Sciences of the United States of America. 2013; 110:E1807–1816. [PubMed: 23620513]

Wisniewski T, Castano EM, Golabek A, Vogel T, Frangione B. Acceleration of Alzheimer's fibril formation by apolipoprotein E in vitro. The American journal of pathology. 1994; 145:1030–1035. [PubMed: 7977635]

Highlights

- ApoE exerts little effects on Aβ accumulation after the initial seeding stage
- Decreasing apoE once fibrils have formed leads to an increase in plaque size
- ApoE4 reduction decreases neuritic dystrophy, independent of Aβ plaque load
- ApoE-targeted therapies aiming to reduce Aβ plaques should focus on prevention

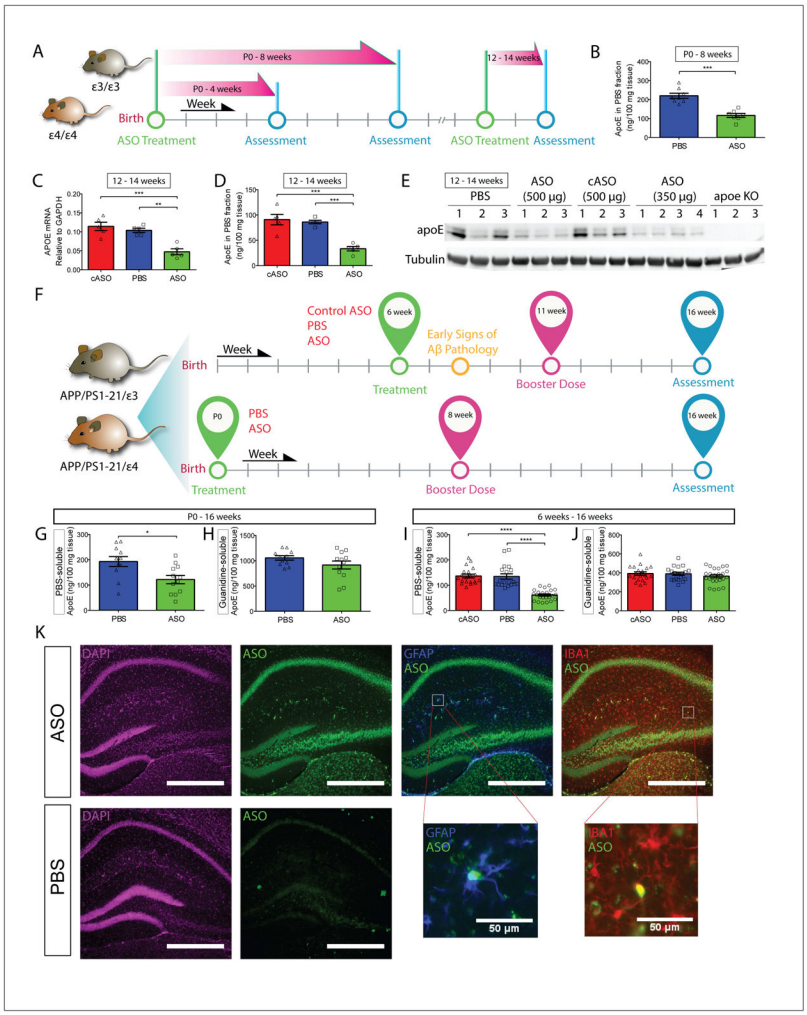

Figure 1. ASO Treatment reduces apoE mRNA and protein levels in APPE4 mice

A, Timeline of various experimental approaches to test for efficacy and optimal dosing of the ASO. ***B,*** E4KI mice were treated with a single bolus of ASO or PBS at P0, and the PBS-soluble apoE levels in the ipsilateral cortex were assessed at 8 weeks (n = 7 – 8 per group, p = 0.0003). ***C,*** 3 – 4 mo E4KI mice were treated with cASO, PBS or ASOs (*n* = 5 per group) and apoE mRNA level in the ipsilateral posterior cortex was analyzed 2 weeks later (p = 0.0002, F = 18.56). ***D***, PBS-soluble apoE levels were measured in brain lysates from the same cohort (p < 0.0001, F = 22.38). ***E,*** Western blot for apoE from the same cohort using anti-apoE antibody HJ15.7. ***F,*** Experimental timelines for APPE4 and APPE3 cohorts. ***G,*** PBS-soluble apoE levels in the contralateral cortex of P0 APPE4 mice were assessed at 4 mo (n = 9 – 12 per group, p = 0.0129). ***H,*** Guanidine-soluble apoE levels in the contralateral cortex were assessed from the same cohort (p = 0.2844). ***I,*** ApoE protein levels in the contralateral cortex from 6wk APPE4 mice were measured via ELISA (n = 20 – 25 per group, p < 0.0001, F = 35.64). ***J,*** Guanidine-soluble *A*poE protein levels were measured from the same set of brain homogenates (p = 0.4316, F = 0.8524). ***K,*** Immunofluorescent staining of ASO- and PBS-treated brains from APPE4 mice. ASOs (green) are taken up by both astrocytes (blue) and microglia (red), as indicated by co-localization with GFAP and

Iba1, respectively. Scale bars = 500 μm, unless otherwise noted. *p < 0.05, **p < 0.01, ***p < 0.001, ****p < 0.0001. All values are reported as mean ± SEM. See also figure S1.

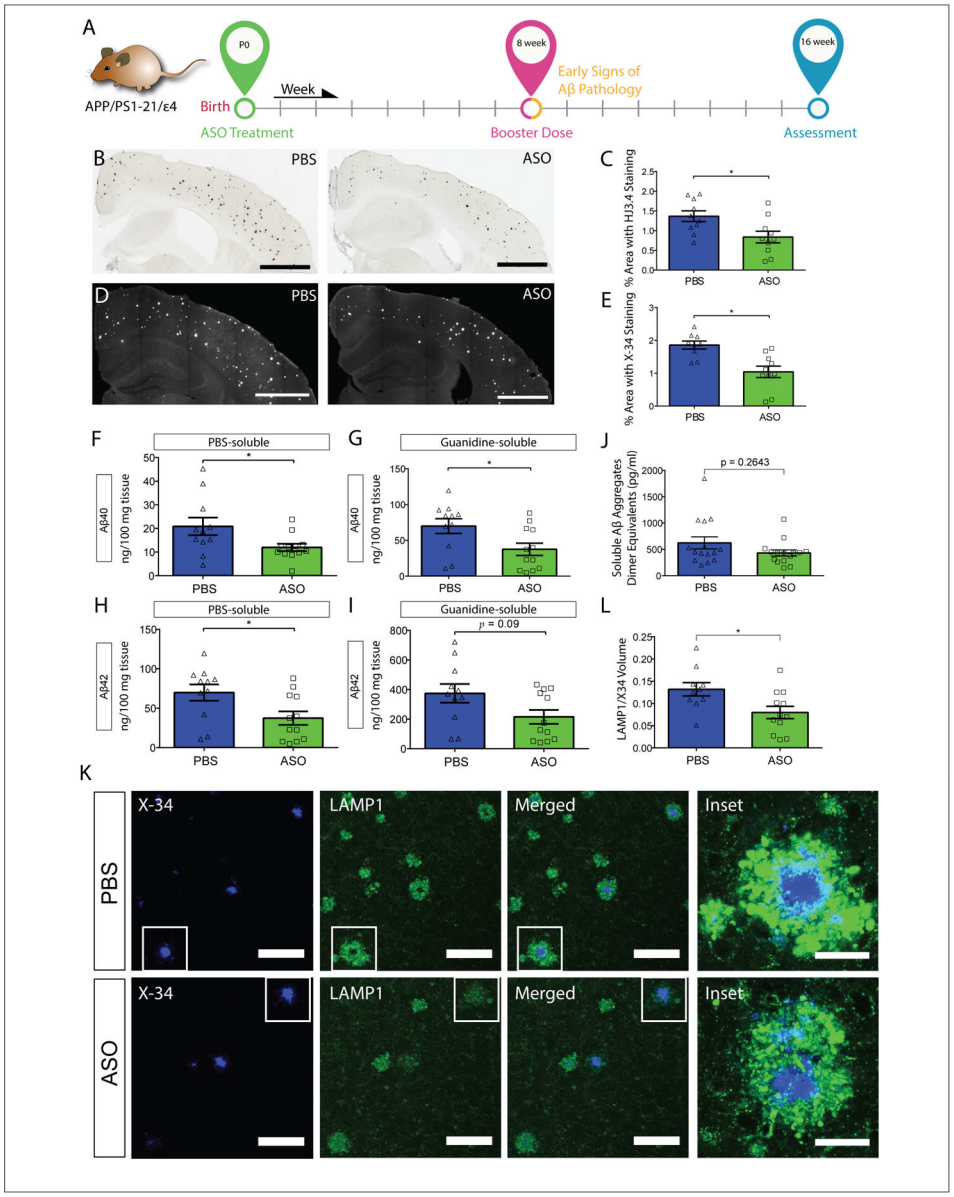

Figure 2. ASO treatment at P0 significantly reduces Aβ plaque pathology in APPE4 mice

A, Experimental timeline for P0 cohort. ***B,*** Brain sections from P0 APPE4 mice treated at P0 were immunostained with anti-Aβ antibody and the extent of Aβ deposition was quantified from the ipsilateral cortex ***(C)*** (Scale bar = 1mm). ***D,*** Brain sections from the same cohort were stained with X-34 dye and the fibrillar plaque load was quantified from the cortex ***(E)*** (Scale bar = 1 mm). PBS-soluble $A\beta_{40}$ ***(F)*** and $A\beta_{42}$ levels ***(H)*** were measured from the contralateral posterior cortex (p = 0.0373 and 0.0129, respectively). Guanidine-soluble $A\beta_{40}$ ***(G)*** and $A\beta_{42}$ levels ***(I)*** were measured from the same cohort (n = 9 – 10 per group, p = 0.0188 and 0.0903, respectively). ***J,*** Oligomeric Aβ levels were measured from PBS-soluble brain lysates (n = 15 per group, p = 0.2643). ***K,*** Representative images of brain sections from P0-treated APPE4 mice co-stained with X-34 and LAMP1. Scale bars = 100 μm. Inset: 60X magnification view of two plaques of similar sizes (one from each treatment group). Scale

bars = 25 μm. ***L***, The volume of LAMP1 staining within 15 μm of an X-34 positive plaque was quantified (n = 10 – 13 per group, p = 0.0196,). *p < 0.05. All values are reported as mean ± SEM. See also figure S2.

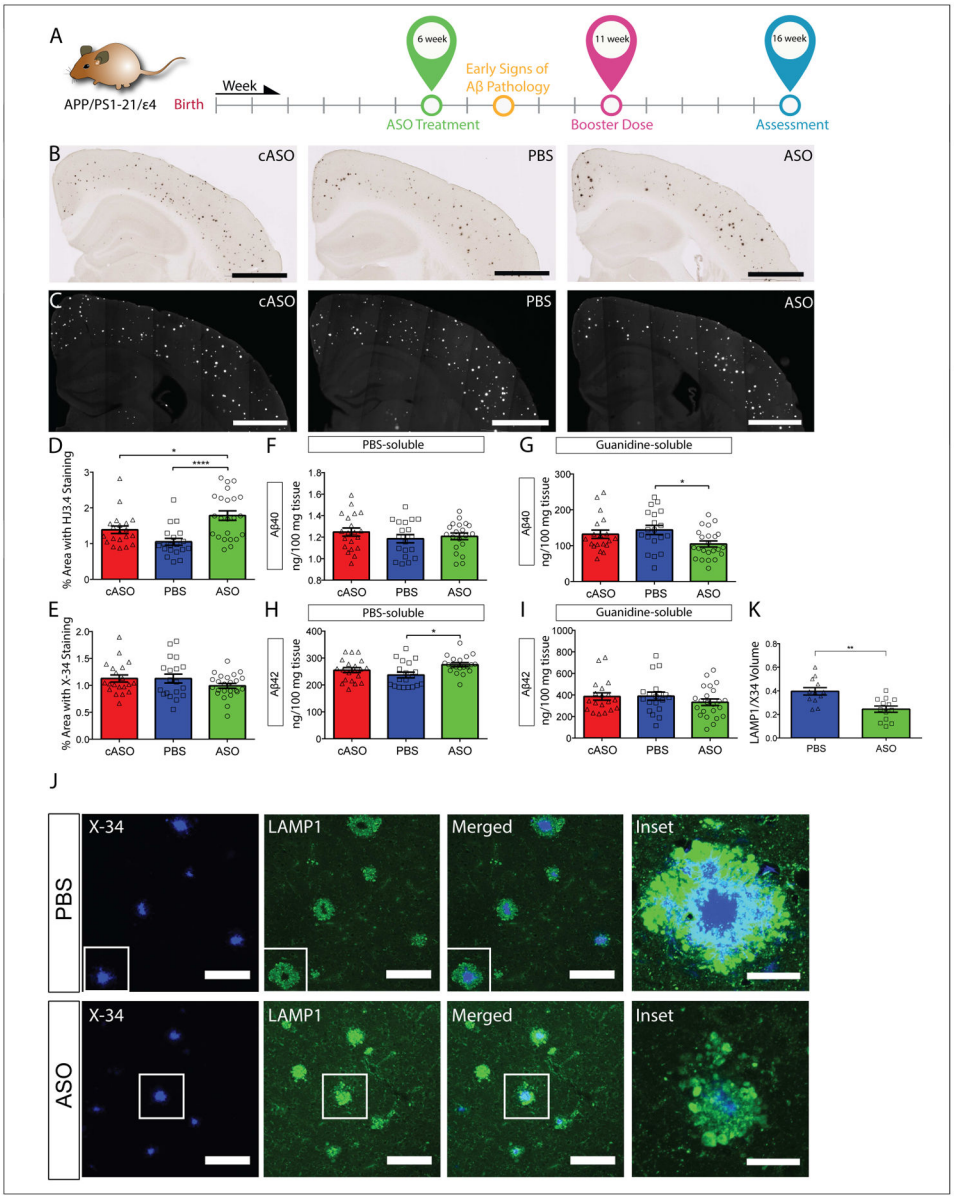

Figure 3. Reduction of apoE expression starting at 6 weeks of age did not significantly alter total Aβ levels in APPE4 mice

A, Experimental timeline for 6wk cohort of APPE4 mice. ***B***, Brain sections from 6wk APPE4 mice were immunostained with an anti-Aβ antibody and the extent of Aβ deposition was quantified from the ipsilateral cortex ***(D)*** ($p = 0.0002$, $F = 10.21$). ***C***. Brain sections from the same cohort were stained with X-34 dye and the fibrillar plaque load was quantified from the ipsilateral cortex ***(E)*** ($p = 0.2095$, $F = 1.604$). Scale bars = 1 mm. PBS-soluble $A\beta_{40}$ ***(F)*** and $A\beta_{42}$ levels ***(H)*** were measured in the contralateral posterior cortex from 4-mo APPE4 mice following 10-weeks treatment (started at 6 weeks of age) with ASO or controls ($p = 0.4673$, $F = 0.7711$ and $p = 0.0171$, $F = 4.379$, respectively). Guanidine-soluble $A\beta_{40}$ ***(G)*** and $A\beta_{42}$ levels ***(I)*** in the contralateral posterior cortex were measured from the same cohort ($p = 0.0326$, $F = 3.635$ and $p = 0.2568$, $F = 1.391$, respectively). N =

20 – 25 per group. ***J,*** Representative images of brain sections from P0-treated APPE4 mice co-stained with X-34 and LAMP1. Scale bars = 100 μm. Inset: 60X magnification view of two plaques of similar sizes (one from each treatment group). ***K,*** The volume of LAMP1 staining within 15 μm of X-34 positive plaques was quantified and normalized to the corresponding X-34 volume (n = 13 per group, p = 0.0019,). *p < 0.05, ****p < 0.0001. Scale bars = 100 μm. All values are reported as mean ± SEM. See also figure S3.

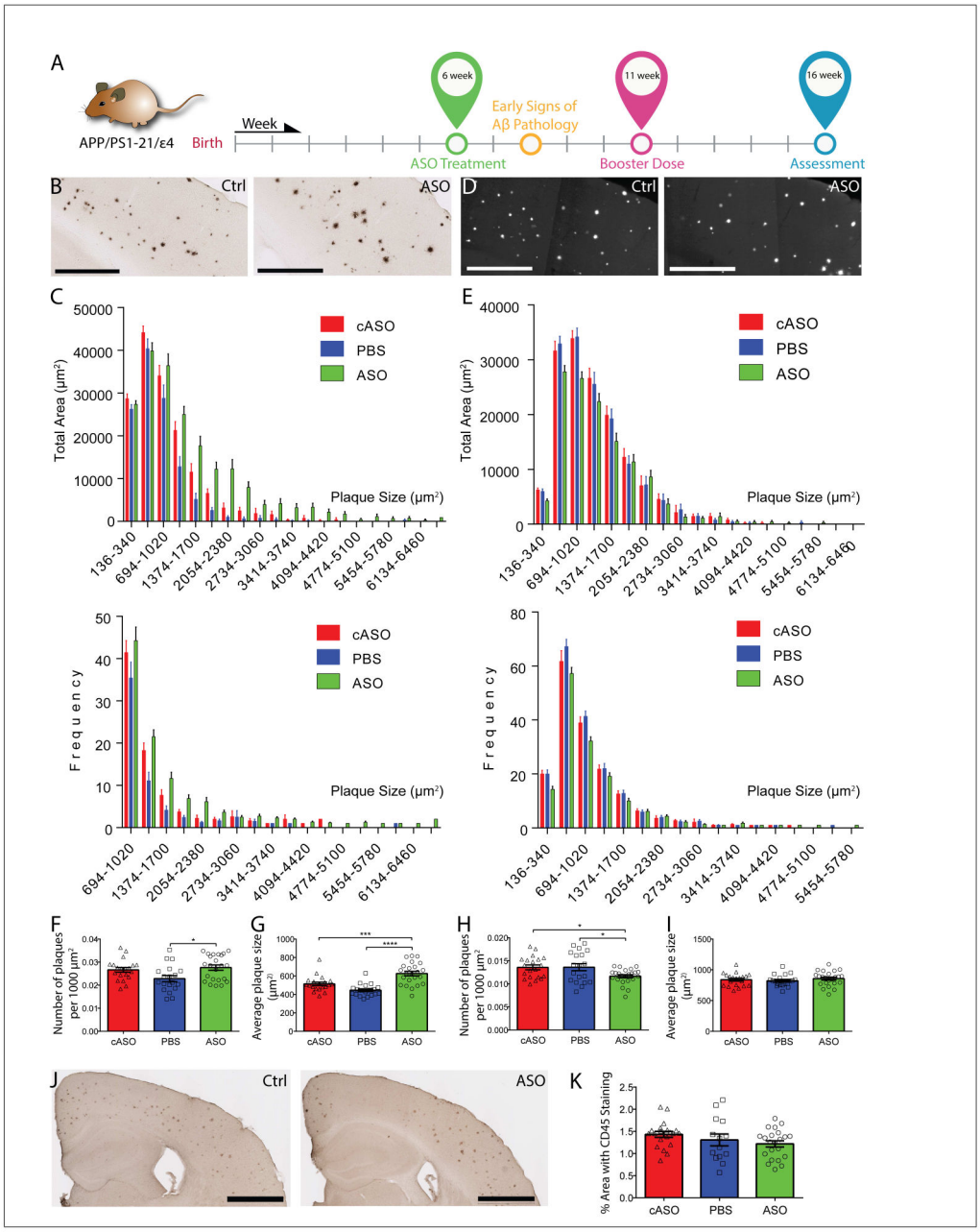

Figure 4. ASO treatment alters plaque size distribution in APPE4 mice

A, Experimental timeline for 6wk cohort***. B,*** Brain sections from APPE4 mice treated with either ASO or cASO stained with anti-Aβ antibody HJ3.4 are shown (Scale bars = 500 μm). Due to space constraints, only the representative images of cASO and ASO were shown. ***C,*** Analysis of the plaque distribution was done by stratifying total plaque coverage based on size, and either the total area covered by plaques of each group (top panel) or the frequency of occurrence (bottom panel) was plotted on the Y-axis. Only plaques larger than 694 μm^2 are shown in bottom panel for clarity. A two-sample K-S test found significant differences in cumulative distribution between cASO and ASO groups (p = 1.39888E-14), as well as between PBS and ASO groups (p = 3.08816E-07). ***D,*** Brain sections from the same cohort

stained with X-34 were shown (Scale bars = 500 μm). ***E,*** Analysis of the plaque size distribution based on X-34 staining was done using a similar approach as in ***(C)***, and the total area covered by plaques of each group (top panel) or the frequency of occurrence (bottom panel) was plotted on the Y-axis. No significant differences in the cumulative distribution of plaques were detected between the groups by the K-S test. The density of Aβ antibody-stained plaques ***(F)*** and average plaque size ***(G)*** was analyzed in the same cohort (n = 20 – 25 per group, $p = 0.0144$, $F = 4.563$ and $p < 0.0001$, $F = 19.80$, respectively). The density of X-34-stained plaques ***(H)*** and average plaque size ***(I)*** was analyzed in the same cohort ($p = 0.0173$, $F = 4.351$ and $p = 0.5839$, $F = 0.5429$, respectively). ***J,*** Brain sections from 4-mo APPE4 mice were immunostained with an antibody against activated microglia, CD45 (Scale bars = 1 mm). ***K,*** The $CD45^+$ area was quantified from the cortex of APPE4 mice (n = 20 – 25 per group, $p = 0.1764$, $F = 1.793$). All values are reported as mean ± SEM. See also figures S4.

KEY RESOURCES TABLE

REAGENT or RESOURCE	SOURCE	IDENTIFIER
Antibodies		
Mouse monoclonal anti-Aβ Antibody HJ3.4	(Bero et al., 2012)	N/A
Mouse monoclonal anti-Aβ Antibody HJ5.1	(Bero et al., 2011)	N/A
Mouse monoclonal anti-$Aβ_{1–40}$ Antibody HJ2	(Bero et al., 2011)	N/A
Mouse monoclonal anti-$Aβ_{1–42}$ Antibody HJ7.4	(Bero et al., 2011)	N/A
Mouse monoclonal anti-apoE Antibody (HJ15.6)	(Liao et al., 2015)	N/A
Mouse monoclonal anti-apoE Antibody (HJ15.7)	(Liao et al., 2015)	N/A
Mouse monoclonal anti-apoE Antibody (HJ15.4)	(Liao et al., 2015)	N/A
Mouse monoclonal anti-Aβ (82E1) Antibody	IBL-America	IBL-America Cat# 10323; RRID:AB_10707424
Rat anti mouse CD45 Antibody	Bio-Rad/AbD Serotec	Cat# MCA1388 RRID:AB_321729
Goat anti-Rat IgG Secondary Antibody, Biotin conjugate	Thermo Fisher Scientific	Cat# PA1-84402 RRID:AB_931503
Rat monoclonal anti-LAMP1 Antibody	Iowa Developmental Studies Hybridoma bank	DSHB # 1D4B
Goat polyclonal anti-iba1 Antibody	Abcam	Abcam # ab5076
GFAP Monoclonal Antibody (GA5), Alexa Fluor 488, eBioscience(TM), Thermo Fisher Scientific	Thermo Fisher Scientific	Cat# 53-9892-82 also 53-9892 RRID:AB_10598515
Rabbit polyclonal anti-pan-ASO Antibody	Ionis Pharmaceuticals	# 13545
Donkey Anti-Mouse Donkey anti-mouse IgG-HRP Polyclonal, HRP Conjugated antibody	Santa Cruz Biotechnology	Cat# sc-2096 RRID:AB_641168
β-Tubulin (H-235) antibody	Santa Cruz Biotechnology	Cat# sc-9104 RRID:AB_2241191
Peroxidase-AffiniPure Goat Anti-Mouse IgG (H + L) antibody	Jackson ImmunoResearch Labs	Cat# 115-035-003 RRID:AB_10015289
Peroxidase-AffiniPure Goat Anti-Rabbit IgG (H+L) antibody	Jackson ImmunoResearch Labs	Cat# 111-035-003 RRID:AB_2313567
Rabbit Anti-Actin Antibody, Unconjugated	Sigma-Aldrich	Cat# A2066 RRID:AB_476693
Purified anti-β-$Amyloid_{1–16}$ antibody,	BioLegend	Cat# 803001 RRID:AB_2564653
Mouse Anti-Human ApoE Monoclonal, Alexa Fluor 647 Conjugated, Clone WUE-4 antibody	Novus Biologicals	Cat# NB110-60531R RRID:AB_1850315
Goat anti-Rat IgG (H+L) Cross-Adsorbed Secondary Antibody, Alexa Fluor 488	Thermo Fisher Scientific	Cat# A-11006 also A11006 RRID:AB_2534074
Streptavidin, Alexa Fluor® 568 conjugate antibody	Thermo Fisher Scientific	Cat# S-11226 RRID:AB_2315774
Donkey Anti-Goat IgG (H+L) Antibody, Alexa Fluor 568 Conjugated	Molecular Probes	Cat# A-11057, RRID:AB_142581
Donkey Anti-Rabbit IgG (H+L) Polyclonal Antibody, Alexa Fluor 647 Conjugated,	Molecular Probes	Cat# A-31573 also A31573 RRID:AB_2536183
Bacterial and Virus Strains		

REAGENT or RESOURCE	SOURCE	IDENTIFIER
Biological Samples		
Chemicals, Peptides, and Recombinant Proteins		
Trizol	Life Technologies	15596026
Ethyl Alcohol	Pharmco-Aaper	11100020S
Sucrose	Sigma-Aldrich	S0389
Albumin, Bovine Fraction V (BSA)	RPI Research Products International	9048-46-86
X-34 dye	Gift from Dr. Robert Mach (Styren et al., 2000)	N/A
Critical Commercial Assays		
Lumigen ECL Ultra (TMa-6)	Thermo Fisher Scientific	# NC024069
Micro BCA Protein Assay Kit	Thermo Fisher Scientific	# 23235
TaqMan™ Universal PCR Master Mix	Thermo Fisher Scientific	# 4304437
High-Capacity RNA-to-cDNA™ Kit	Thermo Fisher Scientific	# 4387406
RNeasy Mini Kit (50)	Quiagen	# 74104
Deposited Data		
Experimental Models: Cell Lines		
Experimental Models: Organisms/Strains		
B6.129P2-$^{Apoetm3(APOE*4)Mae}$ N8	Taconic	1549
B6.129P2-*Apoe*$^{tm2(APOE*3)Mae}$ N8	Taconic	1548
B6-Tg(Thy1-APPswe; Thy1-PS1 L166P)	Gift from Dr. Mathias Jucker (Radde et al., 2006)	MGI:3765351
Oligonucleotides		
Anti-apoE ASO sequence: 5′-GGTGAATCTTTATTAAAC-3′	Ionis Pharmaceuticals, Inc.	N/A
Control ASO sequence: 5′-CCTATAGGACTATCCAGGAA-3′	Ionis Pharmaceuticals, Inc.	N/A
Taqman probe for apoE	Applied Biosystems	Hs00171168_m1
Taqman probe for GAPDH	Applied Biosystems	Mm99999915_g1 Gapdh
Recombinant DNA		

REAGENT or RESOURCE	SOURCE	IDENTIFIER
Software and Algorithms		
Prism	Graphpad Software	Version 6.01; http://www.graphpad.com
Excel	Microsoft	https://products.office.com/en/excel
Imaris 8 & 9	Bitplane	http://www.bitplane.com/software/imaris
ImageJ	NIH	Version 1.48q/1.50 g; https://imagej.nih.gov/ij/
Other		